Longitudinal, 3D in vivo imaging of sebaceous glands by coherent anti-Stokes Raman scattering microscopy –normal function and response to cryotherapy

Published in final edited form as:
J Invest Dermatol. 2015 January ; 135(1): 39–44. doi:10.1038/jid.2014.293.

Longitudinal, 3D *in vivo* imaging of sebaceous glands by coherent anti-Stokes Raman scattering microscopy –normal function and response to cryotherapy

Yookyung Jung, Ph.D.[1,2,‡], **Joshua Tam, Ph.D.**[1,2,‡], **H. Ray Jalian, M.D.**[1,3], **R. Rox Anderson, M.D.**[1,2], and **Conor L. Evans, Ph.D.**[1,2,*]

[1]Wellman Center for Photomedicine, Massachusetts General Hospital, Boston, MA

[2]Department of Dermatology, Harvard Medical School, Boston, MA

[3]University of California, Los Angeles, Division of Dermatology, Los Angeles, CA

Abstract

Sebaceous glands perform complex functions, and are centrally involved in the pathogenesis of *acne vulgaris*. Current techniques for studying sebaceous glands are mostly static in nature, whereas the gland's main function – excretion of sebum via the holocrine mechanism – can only be evaluated over time. We present a longitudinal, real-time alternative – the *in vivo*, label-free imaging of sebaceous glands using Coherent Anti-Stokes Raman Scattering (CARS) microscopy, which is used to selectively visualize lipids. In mouse ears, CARS microscopy revealed dynamic changes in sebaceous glands during the holocrine secretion process, as well as in response to damage to the glands caused by cooling. Detailed gland structure, plus the active migration of individual sebocytes and cohorts of sebocytes were measured. Cooling produced characteristic changes in sebocyte structure and migration. This study demonstrates that CARS microscopy is a promising tool for studying the sebaceous gland and its associated disorders in three-dimensions *in vivo*.

Introduction

Sebaceous glands play a predominant role in the etiology and pathology of *acne vulgaris*, the most prevalent skin disorder affecting over 85% of adolescents and many adults (Bhate and Williams, 2013). Many current therapies for acne (e.g. isotretinoin (Rigopoulos *et al.*, 2010), anti-androgens (Katsambas and Dessinioti, 2010), and photodynamic therapy (Sakamoto *et al.*, 2010)) assert their effects, at least in part, by damaging sebaceous glands and/or suppressing their secretory function. This central involvement of sebaceous glands in acne, as well as the increasing appreciation for the complex neuro-immuno-endocrine

[*]Corresponding author – Address: CNY 149 3.210, 13th St, Charlestown, MA 02129, Evans.Conor@mgh.harvard.edu, Fax: 617-726-4453.
[‡]Contributed equally to this work.

Conflict of Interest
Zeltiq Aesthetics Inc. (Pleasanton, CA) provided study equipment (cooling device) and partial research funding for these experiments. RRA receives a portion of royalties from Massachusetts General Hospital derived from Zeltiq. CLE receives a portion of royalties from the licensing of intellectual property related to CARS microscopy.

functions performed by sebaceous glands, has led to a growing interest in the study of sebaceous gland physiology (Nejati *et al.*, 2013). Of the various currently available investigative techniques, three-dimensional morphometric analysis of sebaceous glands has been found to be especially informative (Hinde *et al.*, 2013). This is typically achieved by confocal microscopy in epidermal whole mounts, which requires *ex vivo* labeling of the glands (e.g. by immunofluorescence) (Hinde *et al.*, 2013), and thus, by necessity, limits the data to a static “snap shot” in time. This limitation is particularly significant since the gland’s main function – the excretion of sebum via the holocrine mechanism – is a dynamic process that can only be evaluated over time. In this study we carried out *in vivo*, label-free longitudinal imaging of individual sebaceous glands using coherent anti-Stokes Raman scattering (CARS) microscopy. CARS microscopy is a non-linear imaging technology that can selectively visualize lipids based on their chemical structure to reveal dynamic changes in sebaceous glands, both during their normal holocrine secretion process, as well as in response to damage caused by cryotherapy. No stains or genetic manipulations are needed for *in vivo* CARS microscopy, making it a promising tool for investigating sebaceous gland biology.

CARS microscopy is a highly sensitive, chemically-selective imaging technique capable of real-time, non-perturbative imaging *in vivo* (Evans et al, 2005). The image contrast in CARS microscopy arises from molecular vibrational modes, such as the CH_2 bonds in lipids. A non-linear Raman technique, CARS uses a pair of laser pulse trains, called "pump" (at a frequency ω_p) and "Stokes" (at a frequency ω_s), whose energy difference is set to correspond to a molecular vibration of interest (Evans and Xie, 2008). The combined pulses generate a beat frequency at $\omega_p - \omega_s$ that can coherently drive specific molecular vibrations. When molecules that contain such vibrations are present in the microscope focal volume, strong emission at a new wavelength, called “anti-Stokes”, is generated at $\omega_{as} = 2\omega_p - \omega_s$ that can be readily collected using standard multiphoton filters and detection schemes (Evans and Xie, 2008). CARS is a multiphoton process, and as such, only generates emission at the objective focal point, enabling threedimensional molecular imaging hundreds of microns deep in tissue (Wright et al, 2007). The turbid tissue environment strongly backscatters the anti-Stokes signal, allowing for highly sensitive imaging of tissue lipids in the cell membrane, cytoplasm, and other structures *in vivo*. (Evans et al, 2005)

CARS is a spectroscopic technique that can be used to quantitatively measure chemical species present in intact tissue (Evans and Xie, 2008). In providing three-dimensional images with different chemical "weightings", CARS and other coherent Raman imaging tools (Freudiger et al, 2008; Saar et al, 2011) can be considered microscopic analogs to spectroscopic MRI, which have sub-micron spatial and video-rate temporal resolution. CARS microscopy is particularly sensitive to lipids, as their long hydrocarbon chains contain a multitude of CH_2 moieties that have strong Raman vibrational modes. These properties have made CARS microscopy an attractive technology for biomedical imaging, with applications including the skin (Evans et al, 2005), the peripheral nervous system (Huff and Cheng, 2007; Jung et al, 2014), and brain (Evans et al, 2007; Fu et al 2008).

In this study we used CARS microscopy to image normal sebaceous glands in mouse ears, before and after cryotherapy. Cryotherapy was an early (mid-1900s) treatment for acne,

traditionally performed by applying liquid nitrogen (−196°C) or a “slush” of frozen carbon dioxide and acetone (−78°C) onto an area with acne until “superficial freezing” was achieved (Dobes and Keil, 1940; Graham, 1975). It has also been reported previously that sebaceous glands are especially sensitive to cooling-induced injury (Gage et al., 1979). For the cryotherapy group in this study, we have applied cooling parameters found to be effective at damaging sebaceous glands, without causing gross cryogenic injury to the surrounding tissue (Gage et al., 1979, Figures S1–S3).

Results and Discussion

Normal sebaceous glands

Using CARS microscopy, sebaceous glands were easily seen due to their high contrast, and were imaged in three-dimensions with subcellular resolution. Intracellular lipid lobules were visible as bright granules within each sebocyte, while nuclei and cell membranes were visible in dark contrast due to their lower lipid content. The CARS images are consistent with the established characteristics of holocrine secretion. Sebocyte progenitor cells residing at the periphery of the gland develop into mature sebocytes, while migrating from the periphery to the central, ductal portion of the gland. These fully mature sebocytes then rupture their cell membranes and release their lipid contents, via the infundibulum (which also contains the hair shaft), ultimately onto the skin surface (Thody and Shuster, 1989). In this study, the CARS signal was weakest in the lipid-poor progenitor sebocytes located along the periphery, becoming stronger in sebocytes in the interior portions of the gland, and strongest at the ductal outlet (Figure 1a, marked “1”). This signal pattern corresponds to the accumulation of lipids in maturing sebocytes as they migrate from the periphery towards the gland duct. Characteristic subcellular structures including lipid granules, nuclei, and cell membranes, were observed to gradually degrade, and were eventually lost in sebocytes immediately adjacent to gland outlets. This corresponds to mature sebocytes undergoing cell death and releasing their lipid contents (Figure 1a, marked “2”). In addition, there was a strong CARS signal along the hair shaft, consistent with a lipid coating (Figure 1a, marked “3”, verified with a lipophilic stain in Figure S4).

Using small tattoos as landmarks, we were able to repeatedly locate individual sebaceous glands over the course of serial imaging sessions carried out for up to two weeks. With this method, we were able to track individual sebocytes within the glands as they migrated towards the gland duct during holocrine secretion (Figure 1 b–d). Individual sebocytes and cohorts of sebocytes were identified in glands over time by their connectivity to adjacent cells, which was maintained throughout the process of sebocyte migration. This connective pattern was maintained, even as the sebocytes’ shape and size progressively changed during migration. The sebocytes migrated at a rate of approximately one cell layer (concentric about the gland outlet) per day. Since each gland consists of roughly 6–8 lipid-containing cell layers, the migration rate observed by CARS microscopy is consistent with previous findings that sebocyte turnover occurs over approximately 7–14 days (Bertalanffy, 1957; Epstein and Epstein, 1966; Plewig and Luderschmidt, 1977). The data presented here marks, to our knowledge, previously unreported sebocyte migration visualization directly observed as it occurs *in vivo*. The ability to monitor holocrine secretion over time – both by detecting

deviations from the normal patterning of CARS signal in sebaceous glands, and by tracking the rate of sebocyte migration – should be a powerful tool for studying the myriad physiologic (e.g. androgen levels) and exogenous (e.g. therapeutic agents) factors that can affect sebaceous gland function. CARS microscopy could be used to investigate many currently unknown aspects of sebaceous gland physiology, e.g. sebocyte migration patterns, spatial and temporal relationships between sebocyte migration and lipid accumulation, and (in combination with other imaging modalities) the real-time interactions between sebocytes and other cells/organisms such as leukocytes or bacteria. In addition to its utility as a research tool, CARS microscopy could also potentially be used in clinical settings to non-invasively monitor sebaceous gland-related disease progression and response to therapy. Adapting CARS microscopy to clinical use will require adjustments in instrumentation (such as miniaturization of device components, and including tissue- stabilizing fixtures), which have been successfully achieved before for other optical imaging systems, e.g. confocal microscopy (Rajadhyaksha et al., 1999; Nehal et al., 2008).

Response to cryotherapy

Individual sebaceous glands were monitored over time to examine their response to cryotherapy (Figure 2). Following a single cold exposure at −8°C, there was a gradual loss of subcellular structures in sebocytes (including nuclei, intracellular lipid granules, and cell membranes), alongside a reduction in lipid-content in each gland (Figure 3). These findings are consistent with previous findings (Gage et al., 1979), as well as our own histologic results (Figure S3). The cooling treatment did not substantially change the lipid composition, as confirmed by Raman spectroscopy (Figure S5). CARS signal along the hair shaft was substantially reduced, and in some cases completely abolished, after cooling treatment (Figures 3, S4). This indicates that lipid excretion into the infundibulum may be halted after cooling.

Sebocyte loss appears to occur first along the periphery of the gland, while the cells in the central portions of the gland persisted the longest. This finding is surprising because lipid-rich cells are thought to be especially susceptible to cryotherapy, due to the propensity of lipids to crystallize at temperatures higher than the water ice-point (Manstein *et al.*, 2008; Quesada-Cortes *et al.*, 2008). This observation would lead one to expect that more mature sebocytes near the gland outlet should be more vulnerable to damage caused by lipid crystallization. The unexpected pattern of cell loss, as well as the low temperature required to induce discernable damage to the sebaceous glands, suggest that other mechanisms besides lipid crystallization may contribute to the damage to sebaceous glands caused by cryotherapy.

CARS microscopy showed that the treated sebaceous glands began showing signs of recovery 1–2 weeks after treatment, which correlates with histology (Figure S3). Post-treatment recovery appeared to occur in a somewhat disorganized manner, with gland features that were observed to deviate from normal. Distribution of sebocytes was discontinuous in some cases, with sebocytes present seemingly at random over different parts of the gland. Unilocular lipid-rich structures, devoid of nuclei or intracellular lipid granules, were often found mid-gland, instead of near the gland duct (Figure 4).

While most of the sebaceous glands were able to recover after cooling treatment, some of the glands never recovered within the course of the experiment (Figure 2), which suggests that some sebaceous glands may be permanently damaged by cooling. Future studies to characterize the glands that do and do not recover following cryotherapy, as well as the post-cooling recovery process, should be helpful for optimizing treatment parameters in our practical aim of improving cryotherapy for *acne vulgaris*.

In this study we have demonstrated, to our knowledge previously unreported, the ability to precisely monitor the dynamic behavior of sebaceous glands *in vivo* longitudinally, with subcellular resolution, and without the need for exogenous labeling or genetic manipulation. This capability of CARS microscopy makes it a promising tool for studying the sebaceous gland and its associated disorders. We have directly measured sebocyte migration, and the effects of a cold cycle on sebaceous glands *in vivo* using CARS. Surprisingly, this study revealed sensitivity of sebocytes at the gland periphery to cold injury. We also determined the recovery of a population of glands.

In addition to monitoring sebaceous glands with CARS microscopy alone, as we demonstrated in this study, additional imaging modalities could be combined with CARS for even more comprehensive studies, especially for disease models. Two of the most prevalent disorders involving sebaceous glands – *acne vulgaris* and rosacea – both involve additional factors besides sebocytes themselves: colonization by *propionibacterium acnes* in acne, and dysfunction of the local vascular system in rosacea. Combining the monitoring of sebocytes by CARS microscopy with quantitative imaging of these related factors is likely to yield additional mechanistic insights into these disorders and contribute significantly to the development of effective therapies.

Materials & Methods

Animals

All animal procedures were performed in compliance with the Public Health Service Policy on Humane Care and Use of Laboratory Animals, and approved by the Massachusetts General Hospital Institutional Animal Care and Use Committee. The mouse ear model was chosen for this study because of its high density of sebaceous glands, as well as ease of access. Adult female BALB/c mice (12–16 weeks old) purchased from Jackson Lab (Bar Harbor, ME) were used for all experiments. During cooling and microscopy procedures the animals were anesthetized by inhaled isoflurane (1–3%). For cooling treatment, the ear was placed upon a conductive cooling plate, and held in place by an insulation block weighing 100g. Temperature in the cooling plate was maintained by computer-controlled thermoelectric coolers. The treated ears were held against the cooling plate at −8°C for 10 minutes each. Untreated ears were used as controls. Small tattoos were placed in the ears to serve as landmarks, so that the same sebaceous glands can be identified and imaged repeatedly over the course of the study. 5 treated and 4 control animals were imaged in this manner, with 3–4 glands in each animal imaged at various intervals. For microscopy, the ear being examined was flattened and secured to a glass coverslip using a thin layer of methyl cellulose solution (Fisher Scientific, Pittsburgh, PA).

CARS Microscopy

The excitation light for CARS microscopy was generated using a pair of high repetition rate, low pulse power infrared lasers for deep, non-perturbative imaging in skin *in vivo*. (Evans et al, 2005) Briefly, a 7 ps, 1064 nm, mode-locked Nd:Vanadate laser (PicoTRAIN, High-Q Laser) was used to synchronously pump an optical parametric oscillator (OPO) (Levante, APE) that produced wavelength-tunable 3 ps duration pulses. A portion (500 mW) of the 1064 nm output was used as the Stokes beam. For imaging of the lipid-rich sebum, the pump beam from the OPO was tuned between 814 and 816 nm to be in resonance with methylene stretching vibrations. The pump and Stokes pulse trains were combined using a 950 short pass dichroic mirror (Chroma Technology) and overlapped in time using a delay line.

The combined pump and Stokes beam were steered into the infrared side port of a modified Olympus FV1000 confocal laser scanning microscope. The beam was aligned through the microscope as described elsewhere (Jung et al, 2012). A UPlanSApo 20× 0.75NA objective was used as the objective lens for all experiments. The epi-collected anti-Stokes emission was passed through a 650 nm, 25 nm bandpass filter (Chroma Technology) and focused onto a Hamamatsu H7422PA-40 photomultiplier tube. The current output of the photomultiplier tube passed through a high-speed current amplifier (Femto, HCA-4M-500K) and was detected using Olympus input/output hardware. Images were acquired using the built-in Olympus FV10 software.

Images were collected at standard acquisition rates (2 sec/frames, 2 us per pixel, Kalman averaging of 3) using approximately 30 mW of pump and 35 mW of Stokes power at the focus. Animals were examined following imaging sessions to look for evidence of tissue perturbation, including redness or swelling. No signs or symptoms of tissue damage or perturbation were observed. Animals were mounted on a motorized state (Prior, H117 stage) with 0.01 μm resolution, which enabled precise and repeatable imaging of sebaceous glands over the course of days and weeks. Near-infrared light that passed through the thin mouse ear was collected on the microscope's transmission detector to create transmission images.

Supplementary Material

Refer to Web version on PubMed Central for supplementary material.

Acknowledgments

We thank Sunny Xie and Dan Fu of Harvard University for allowing the use of the Raman microscope. This study was funded, in part, by R21CA53335 (CLE) and a New Innovator Award (DP2 OD007096, CLE). Information on the New Innovator Award Program is at http://nihroadmap.nih.gov/newinnovator/.

Abbreviations used

CARS coherent anti-Stokes Raman scattering

References

Bertalanffy FD. Mitotic activity and renewal rate of sebaceous gland cells in the rat. Anat Rec. 1957; 129:231–241. [PubMed: 13509193]

Bhate K, Williams HC. Epidemiology of acne vulgaris. The British journal of dermatology. 2013; 168:474–485. [PubMed: 23210645]

Dobes WL, Keil H. Treatment of acne vulgaris by cryotherapy (slush method). Arch Derm Syphilol. 1940; 42:547–558.

Epstein EH, Epstein WL. New Cell Formation in Human Sebaceous Glands. J Invest Dermatol. 1966; 46:453–458.

Evans CL, Potma EO, Puoris'haag M, et al. Chemical imaging of tissue in vivo with video-rate coherent anti-Stokes Raman scattering microscopy. Proc Natl Acad Sci U S A. 2005; 102:16807–16812. [PubMed: 16263923]

Evans CL, Xie XS. Coherent anti-stokes Raman scattering microscopy: chemical imaging for biology and medicine. Annual review of analytical chemistry. 2008; 1:883–909.

Evans CL, Xu X, Kesari S, et al. Chemically-selective imaging of brain structures with CARS microscopy. Optics express. 2007; 15:12076–12087. [PubMed: 19547572]

Freudiger CW, Min W, Saar BG, et al. Label-free biomedical imaging with high sensitivity by stimulated Raman scattering microscopy. Science. 2008; 322:1857–1861. [PubMed: 19095943]

Fu Y, Huff TB, Wang H-W, et al. Ex vivo and in vivo imaging of myelin fibers in mouse brain by coherent anti-Stokes Raman scattering microscopy. Optics express. 2008; 16:19396–19409. [PubMed: 19030027]

Gage AA, Meenaghan MA, Natiella JR, et al. Sensitivity of pigmented mucosa and skin to freezing injury. Cryobiology. 1979; 16:348–361. [PubMed: 487851]

Graham GF. Cryosurgical treatment of acne. Cutis. 1975; 16:509–513.

Hinde E, Haslam IS, Schneider MR, et al. A practical guide for the study of human and murine sebaceous glands in situ. Experimental dermatology. 2013; 22:631–637. [PubMed: 24079731]

Huff TB, Cheng JX. In vivo coherent anti-Stokes Raman scattering imaging of sciatic nerve tissue. J. Microsc. 2007; 225:175–182. [PubMed: 17359252]

Jung Y, Nichols AJ, Klein OJ, et al. Label-Free, Longitudinal Visualization of PDT Response In Vitro with Optical Coherence Tomography. Israel journal of chemistry. 2012; 52:728–744. [PubMed: 23316088]

Jung YK, Ng JH, Keating CP, et al. Comprehensive Evaluation of Peripheral Nerve Regeneration in the Acute Healing Phase Using Tissue Clearing and Optical Microscopy in a Rodent Model. Submitted. 2014

Katsambas AD, Dessinioti C. Hormonal therapy for acne: why not as first line therapy? facts and controversies. Clin Dermatol. 2010; 28:17–23. [PubMed: 20082945]

Manstein D, Laubach H, Watanabe K, et al. Selective cryolysis: a novel method of non-invasive fat removal. Lasers Surg Med. 2008; 40:595–604. [PubMed: 18951424]

Nehal KS, Gareau D, Rajadhyaksha M. Skin imaging with reflectance confocal microscopy. Semin Cutan Med Surg. 2008; 27:37–43. [PubMed: 18486023]

Nejati R, Skobowiat C, Slominski AT. Commentary on the practical guide for the study of sebaceous glands. Experimental dermatology. 2013; 22:629–630. [PubMed: 24079730]

Plewig G, Luderschmidt C. Hamster ear model for sebaceous glands. J Invest Dermatol. 1977; 68:171–176. [PubMed: 845450]

Quesada-Cortes A, Campos-Munoz L, Diaz-Diaz RM, et al. Cold panniculitis. Dermatol Clin. 2008; 26:485–489. vii. [PubMed: 18793981]

Rajadhyaksha M, Anderson RR, Webb RH. Video-rate confocal scanning laser microscope for imaging human tissues in vivo. Applied optics. 1999; 38:2105–2115. [PubMed: 18319771]

Rigopoulos D, Larios G, Katsambas AD. The role of isotretinoin in acne therapy: why not as first-line therapy? facts and controversies. Clin Dermatol. 2010; 28:24–30. [PubMed: 20082946]

Saar BG, Freudiger CW, Reichman J, et al. Video-rate molecular imaging *in vivo* with stimulated Raman scattering. Science (New York, NY). 2010; 330:1368–1370.

Sakamoto FH, Lopes JD, Anderson RR. Photodynamic therapy for acne vulgaris: a critical review from basics to clinical practice: part I. Acne vulgaris: when and why consider photodynamic therapy? J Am Acad Dermatol. 2010; 63:183–193. quiz 93–4. [PubMed: 20633796]

Thody AJ, Shuster S. Control and function of sebaceous glands. Physiol Rev. 1989; 69:383–416. [PubMed: 2648418]

Wright AJ, Poland SP, Girkin JM, et al. Adaptive optics for enhanced signal in CARS microscopy. Optics express. 2007; 15:18209–18219. [PubMed: 19551119]

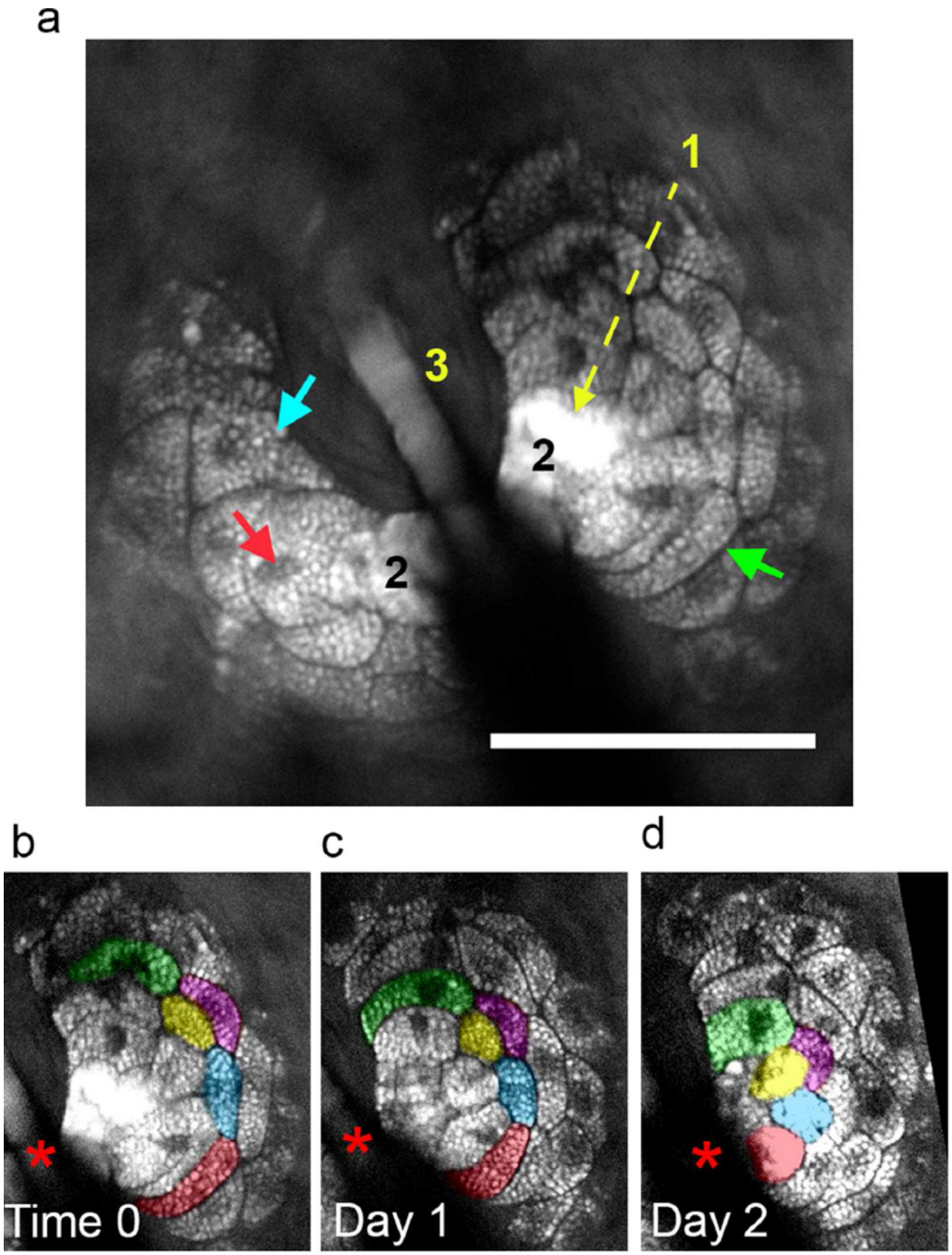

Figure 1.

CARS imaging of normal sebaceous glands. (a) A sebaceous gland showing intracellular lipid granules (blue arrow), nuclei (red arrow) and cell membranes (green arrow). (1) CARS signal intensity increases as sebocytes approach the gland duct, corresponding to lipid accumulation as sebocytes mature. (2) Sebocytes near the duct show the highest CARS signal and lose cellular structures corresponding to cell death and lipid content release. (3) Hair shafts are coated with secreted lipid. (b–d) Sebocyte migration in the same sebaceous gland shown in (a) over 3 consecutive days. Five sebocytes are marked in separate colors to

facilitate identification. As the sebocytes migrated to the gland duct (*), there is a loss in intracellular structures and a concomitant increase in CARS signal. Scale bar: 50 μm.

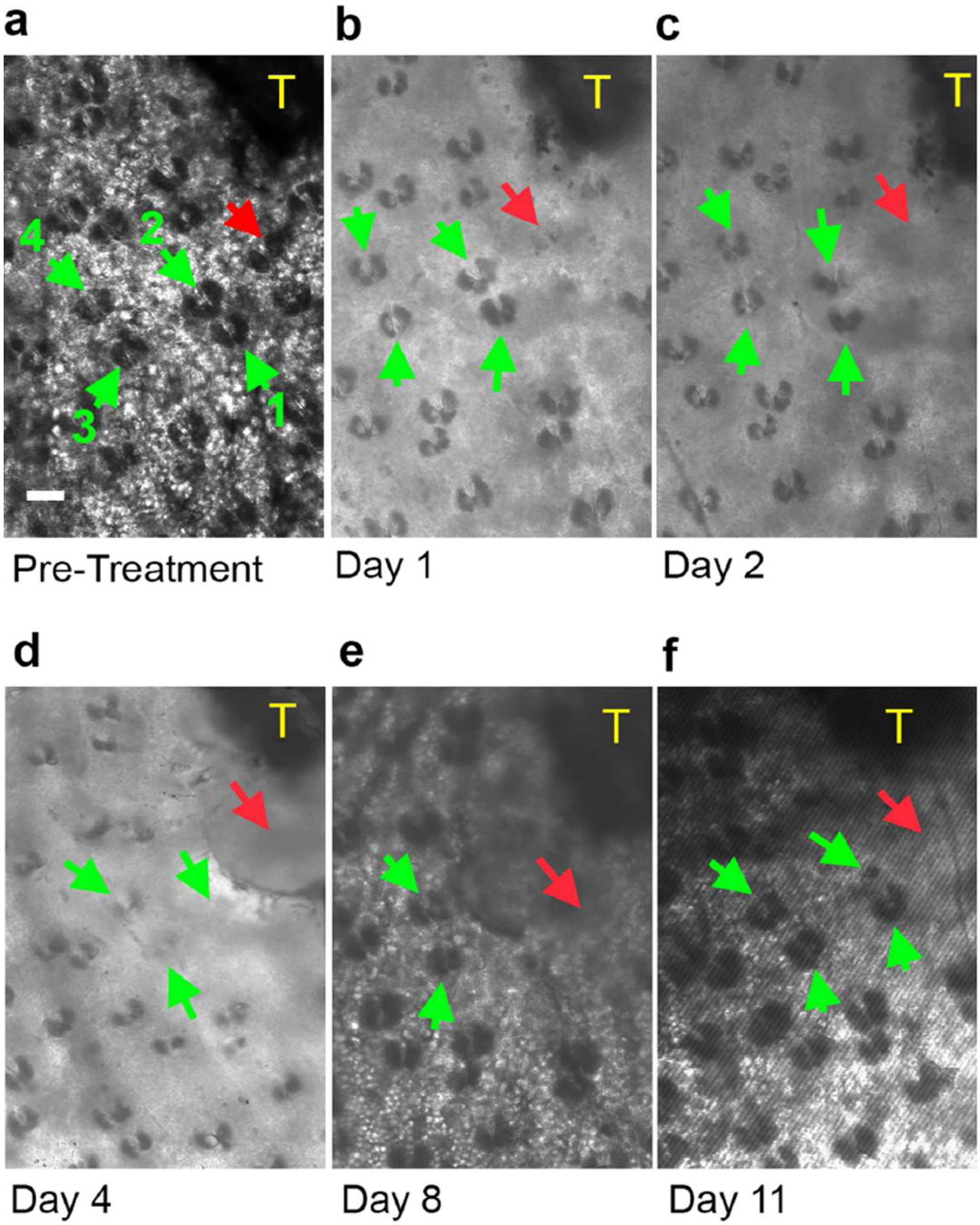

Figure 2.

Transmission microscopy images of sebaceous glands before and after cryotherapy. A tattoo (T) was used as a landmark so that the same sebaceous glands could be identified across different imaging sessions. Four sebaceous glands (green arrows) were randomly chosen for longitudinal monitoring. Changes in overall gland structure can be seen after cooling. Most glands appeared to recover eventually, but a few were unable to recover within the study period (one such gland marked by red arrow). The “grainy” background in images taken pre-treatment and at later time points is caused by light transmitting through the subcutaneous

fat. The clearing of this background in early post-treatment days is likely due to changes in tissue refractive index caused by transient edema. Scale bar: 100 μm.

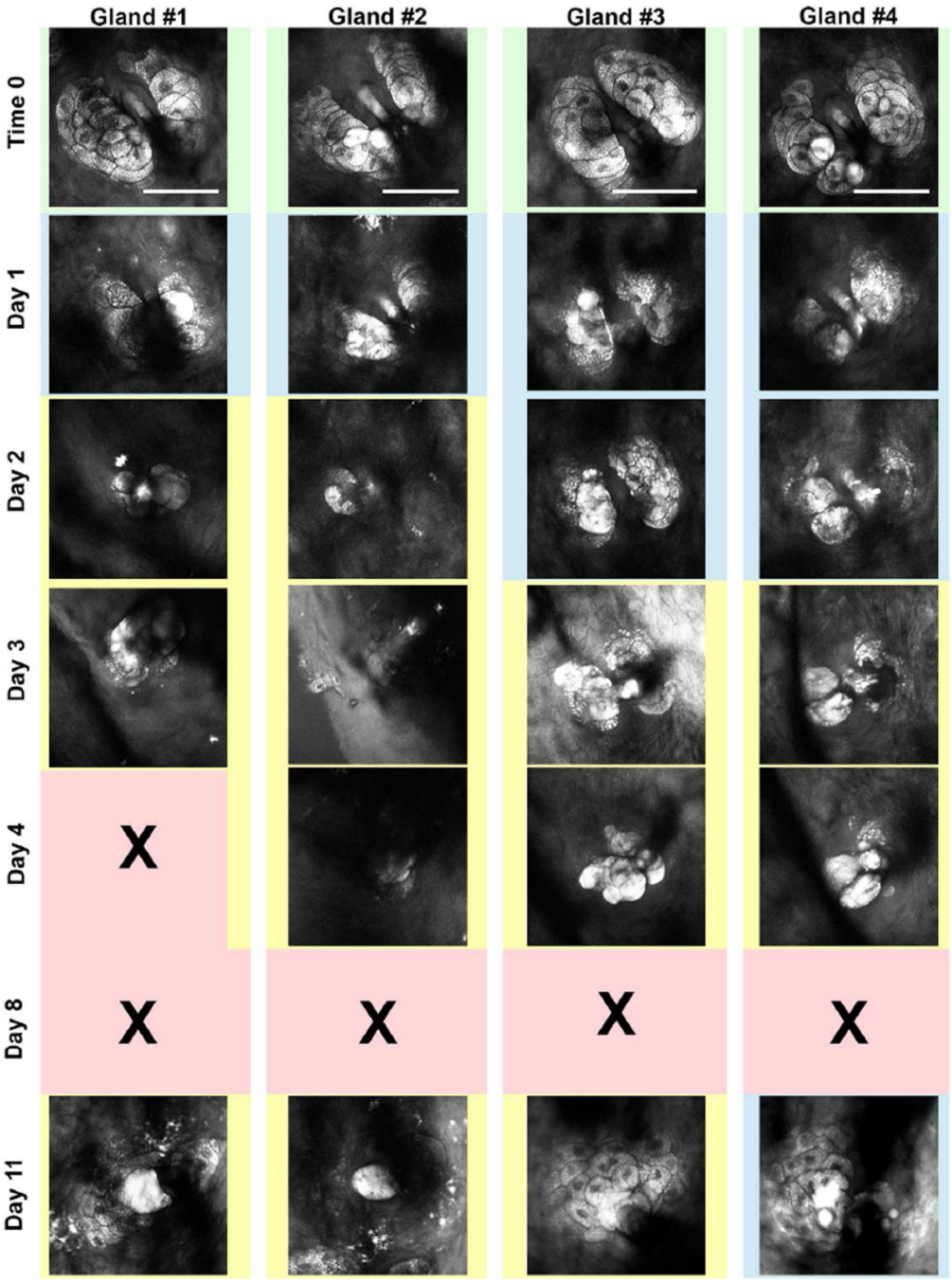

Figure 3.

CARS images of 4 individual sebaceous glands (marked by green arrows in Figure 2) at different times post-cooling, showing both damage to gland structures and subsequent recovery. Green background denotes glands with normal morphology. Blue background denotes glands showing damage to intracellular structures, while the general gland structure remained relatively intact. Yellow background denotes glands showing severe damage, with major disruption in overall gland structure. Red background denotes time points where CARS signal could not be detected. Scale bars: 50 μm.

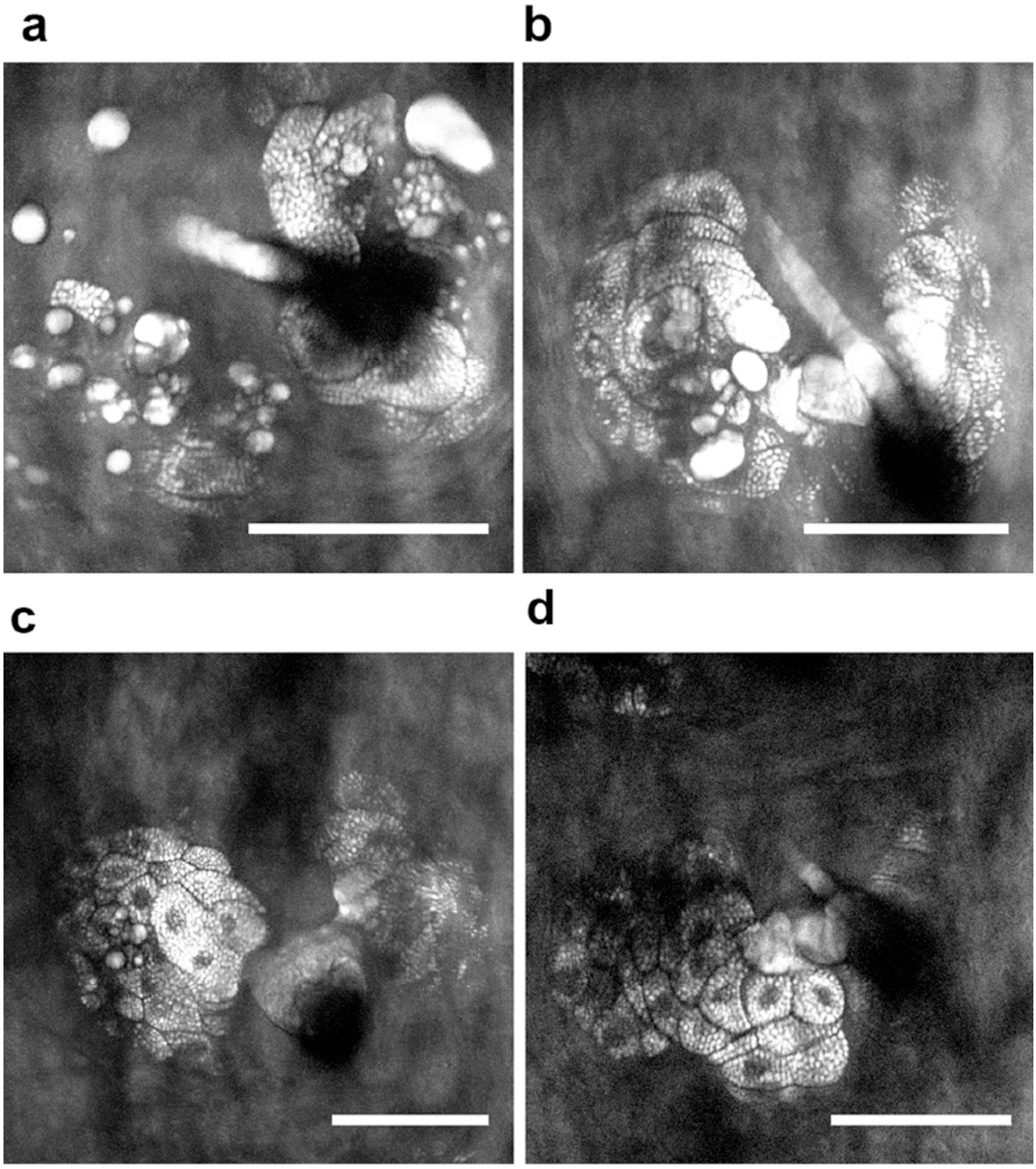

Figure 4.

Sebaceous glands at various stages of recovery, showing abnormal gland features such as discontinuous distribution of sebocytes, with sebocytes present seemingly at random over different parts of the gland (a); presence of unilocular lipidrich structures, devoid of nuclei or intracellular lipid granules in middle-peripheral portions of the gland, instead of near the gland duct (a, b, c). Other glands were able to recover normal gland features at the same time point (d). All glands were imaged at 8 days post-cooling. Scale bars: 50 μm.